International Journal of Latest Engineering Research and Applications (IJLERA) ISSN: 2455-7137

Volume – 10, Issue – 04, April 2025, PP – 36-48

Impact of a Transverse Crack of the Shaft on Dynamic Stiffness

P. Fraga,[1] F. De Cal, B.[2]

[1]*PhD Mechanical Engineer, A Coruña University. Spain*
Higher Polytechnic School, Department of Industrial and Naval Engineering
C./Mendizabal s/n 15403 Ferrol (A Coruña), Spain
[2]*PhD Mechanical Engineer, MSc Sustainable Energy Systems of Queen Mary University of London*

Abstract: A rotor of laboratory model of 2 degrees of freedom, with solid bronze bearings, has been studied to which a transverse crack of 10% of the shaft diameter, approximately, has been made, in addition to introducing a determined mass imbalance and a vertical radial load to cause the propagation of this crack. The rotor in question is horizontal, so the force of gravity will also act and add to the vertical load for the propagation of that crack.

It is observed how the 1X and 2X responses are increased and stand a method to detect a crack in the shaft. The relationships between both responses remain considered and are fundamental as a symptom of the crack, as well as others. However, in this work we had concentrated on what the crack means for the modification, decrease in this case, of the dynamic stiffness of the shaft in its stands, measured through two induction or proximity transducers in order to verify the clear difference between the shaft containing the crack and another installed perpendicular to the latter.

Keywords: Rotor dynamics, shaft crack, dynamic stiffness.

1. Introduction

The mathematical model of motion is as follows, equation (1),which corresponds to the cross-section of the shaft of the Figure 1, where "m" is the mass of the rotor, "h" is the eccentricity of the mass, "g" is the acceleration of gravity, "d" is the damping coefficient of the shaft, "k_η" and "k_ξ" are the stiffness of the shaft in the directions of the crack and perpendicular to the crack respectively, "$k_{\xi\eta}$" and "$k_{\eta\xi}$" are the coupling stiffness of both axes, "ω" is the rotational speed and "δ" is the angle between the center of gravity and the geometric center, "C" the center of gravity; e_η = rotor shaft stiffness offset. The shaft has smaller stiffness in "η" axis direction (which is the crack direction) than "ξ" axis direction (ξ, η are rotating axis, x, y are fixed inertial axes). [1]

$$\begin{aligned} m\left(\ddot{\xi} - 2\omega\dot{\eta} - \omega^2\xi\right) + d\left(\dot{\xi} - \omega\eta\right) + v_\xi^2\xi &= mh\omega^2\cos(\delta+\theta) - mg\sin\omega t \\ m\left(\ddot{\eta} - 2\omega\dot{\xi} - \omega^2\eta\right) + d(\dot{\eta} + \omega\xi) + v_\eta^2\eta(1-\Delta)\left[1 + \frac{\varepsilon}{2}(sign\ of\ "\eta" - 1)\right] & \\ = mh\,\omega^2\sin(\delta+\theta) - mg\ \cos\omega t - v_\eta^2 e_\eta & \end{aligned} \quad (1)$$

The parameters Δ, ε are the gaping and breathing crack, respectively, which modifies the natural frequency by increasing the asymmetry of the shaft also, by the appearance of a non-linear effect such as the sign of "η", while $v_\xi = \sqrt{k_\xi/m}$, $v_\eta = \sqrt{k_\eta/m}$ are natural frequencies of the rotor.

The shaft section is not symmetrical as a result of the crack; its main axes of inertia are Pξ1 and Pη1(Figure 1) and the rotating axes ξ and η are positioned parallel to ξ1 and η1. Consequently, the main axis of inertia, Pξ1, is perpendicular to the other axisPη1, which contains the crack.

The center of gravity "C" of the disk is located at the distance OC=h. The angle "θ" is the measure of the shaft cross section principal between the shaft higher rigidity axis "ξ" and the reference axis of the disk OR, which is located vertically when the key phasor probe and the shaft key phasor corresponded.

We consider a shaft with a unbalanced disk rotating to constant angular speed ω, which have equal stiffness in the two directions x, y: $k = k_x = k_y$. The shaft section with crack is not symmetric and its principal axes of inertia are $P\xi_1$and $P\eta_1$. The center of mass of the shaft rises in the Figure 1, the value marked e_η, due to this displacement the asymmetry in the stiffness with respect to both axes is to be expected$P\xi_1$ and $P\eta_1$,which is[2]:

$$k_\xi = \frac{1}{\frac{1}{k} + \frac{l^3}{12EI_\xi}};\ k_\eta = \frac{1}{\frac{1}{k} + \frac{l^3}{12EI_\eta}}$$

I_ξ and I_η are inertia moments of the shaft cross section about $\xi 1$ and $\eta 1$, E is the Young module.

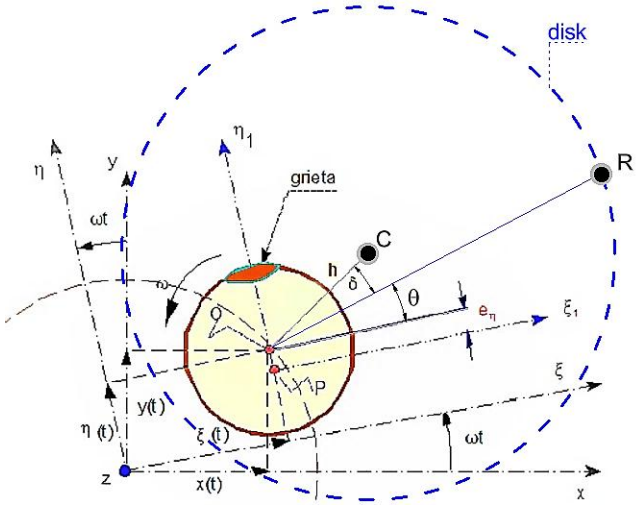

Figure 1: Section shaft with crack

An important characteristic of the transverse crack in the shaft, which differentiates it from the presentation of the misalignment, is that the crack also has two simultaneous 1X and 2X responses, because the crack creates an internal force, due to that asymmetry of the moments of inertia, which rotates with the shaft and therefore manifests itself in all planes, not just in the plane that is misaligned. Hence the importance of installing two transducers at 90º, to detect two directions.[3]

Recent studies are already focused on the effect on the life cycles of the elements of a bearing, due to the modification of the angle of inclination that occurs (Lodz University of Technology, Department of Dynamics, Poland) [4]. Other studies also analyse the connection of the phenomena of imbalance, misalignment and cracks in the shaft, its initiation and propagation between different couplings of rotors (Department of Mechanical Engineering, University of Alberta, AB, Canada) [5].

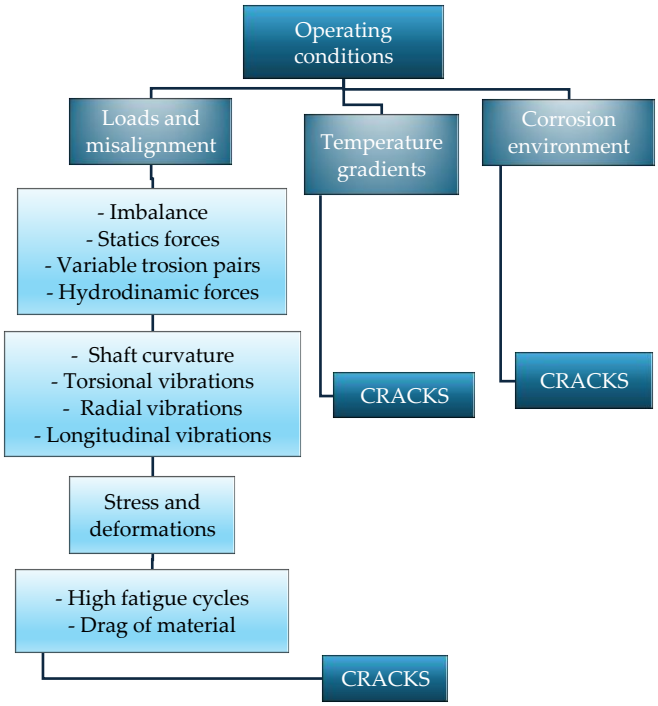

Figure 2: Causes related to cracking in a shaft

2. Experiment and Case Study

A test is carried out on a study rotor, such as the one in Figure 3. 90º induction transducers are also installed in the (x) and (y) axes and another for phase reference (key-phasor), as well as seismic transducers or accelerometers on the pedestal, although really, the decision to use one or the other transductor depends a lot on the relative stiffness of the bearings [6].

The dimensions of the rotor-kit are 165 x 340 x 789 mm, shaft diameter of 9,5 mm and maximum speed of 6000 rpm, with bronze bearing. It also has a coupling device to the shaft that constitute a mechanical seal in a pressurized fluid environment contained in a transparent polycarbonate shell and its accessories.

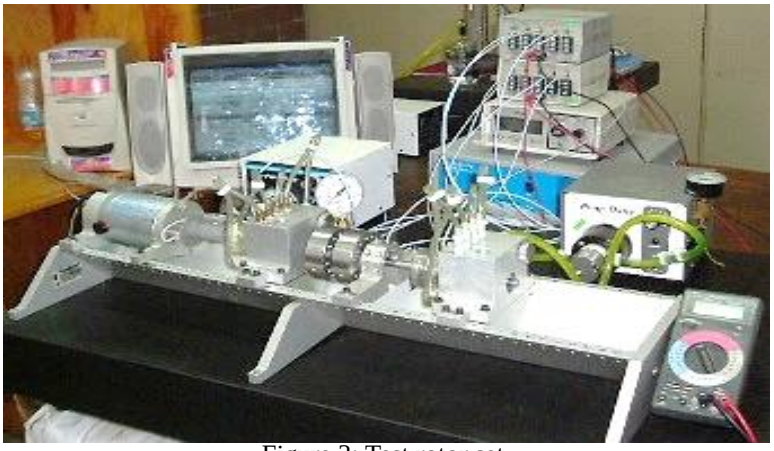

Figure 3: Test rotor set

The dynamic system of rotation that is analysed can be assimilated to the possible failures in a rotor of tests like the Figure 3[7], and that it is chosen to know from it its mechanical characteristics in order to perform and obtain real numerical calculations, on that model, which will always be more explicit. It consists of a mechanical foundation that includes a dc-electric drive motor, a shaft-rotor with test discs, bronze bearings, six magnetic induction transducers, three probe assemblies and a safety cover of polycarbonate.

Instrumentation and equipment are also available, such as:

- Spectrum analyser with 208-P data acquisition unit, computer and analyser software with graphic presentation of vibrations for Windows. The graphs that this analyser displays on the computer are shaft orbits, diagrams on the basis of time, trend diagrams, XY graphs, vector tabulation, Ny quist polar diagrams, Bode diagrams, shaft centre position and cascade spectra.
- Digital vector filter for selection of responses to the different frequencies' disturbance.
- Two oscilloscopes for analysis of the position of the shaft centre.
- Speed control instrumentation, oil pump, cooling system, two thermometers.
- Laser aligner "Easy Laser Shims".
- Brookfield digital Viscometer.
- Manometer from 0 to 700 kPa,
- and another phase reference, plus a load spring frame to simulate shaft eccentricities.

The model of rotor to perform this test, is indicated in the plot of Figure 4, in which a transverse crack of 6 mm has been made, as a first step, where: 1.- is a 75W cc drive motor, 2.- flexible coupling, 3a and 3b.- antifriction/bronze bearings, 4.- 1,63 kg disc-rotor, 5.- shaft centring support with four springs, 6.- aluminium disc for controlled imbalances, 7.- mechanical seal of 50 mm in length with radial clearance of 220μm and a circuit pressure of 10342 Pa, 8.- pressurized oil circuit in the gap of the seal, 9.-mechanical seal horizontal and vertical induction transducers,11.-axial transducer, so phase reference transducer and seismic transducer.

The characteristics of this test rotor, before making the crack in the shaft, that were calculated as indicated [8], are:

- Natural rotor frequency, without crack, 2180 rpm.
- Modal stiffness coefficient, K = 18,26 KN/m.

In the model of the Figure 4 has been assumed that only the disk has mass, neither the shaft nor other elements. In the real rotor add some mass furthermore to the disk.

The dynamic phenomena linked with a cross crack in the shaft are related to a decrease of the shaft stiffness in the direction of the crack and rotating with this shaft. The stiffness coefficients in two directions are now different due to the unequal value of the moment of inertia with the crack and, on the other hand, the stiffness axis (which is the one that unites the centres of gravity of the masses) not the same with the crack as the axis of rotation and an imbalance of mass occurs, similar to a bent shaft according to Figure 5. [9]

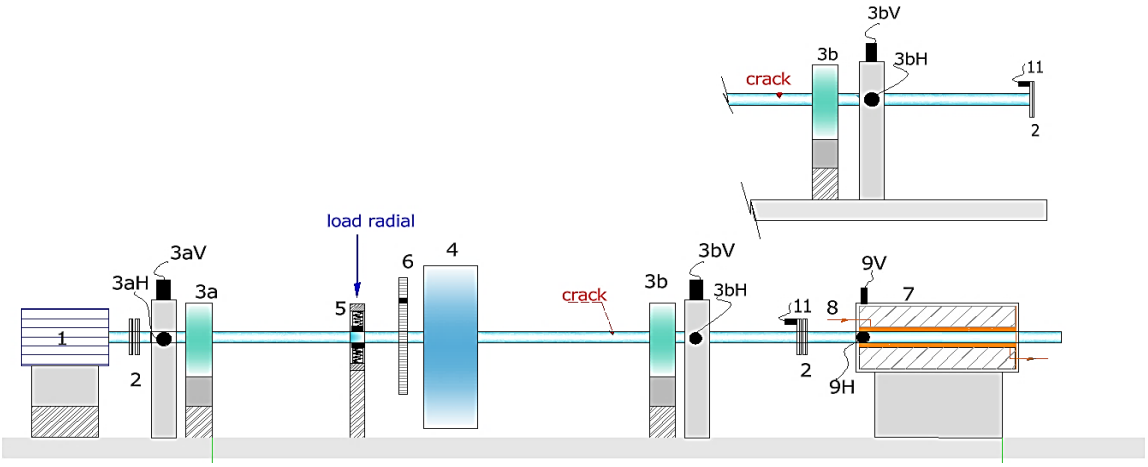

Figure 4: Rotor kit with crack

According to this Figure 5, there are several aspects to highlight: first, the location of the center of the shaft will be in the same quadrant, both lower or both higher; second, the normal force "N" will be opposite on both sides of the crack, so there will be hardly any axial vibration, they are compensated; third, the "R" force that is exerted on the shaft due to the tilt of the crack, rotates with the shaft, so it will appear in all directions; and fourth, the stiffness only decrease in the direction of the crack.

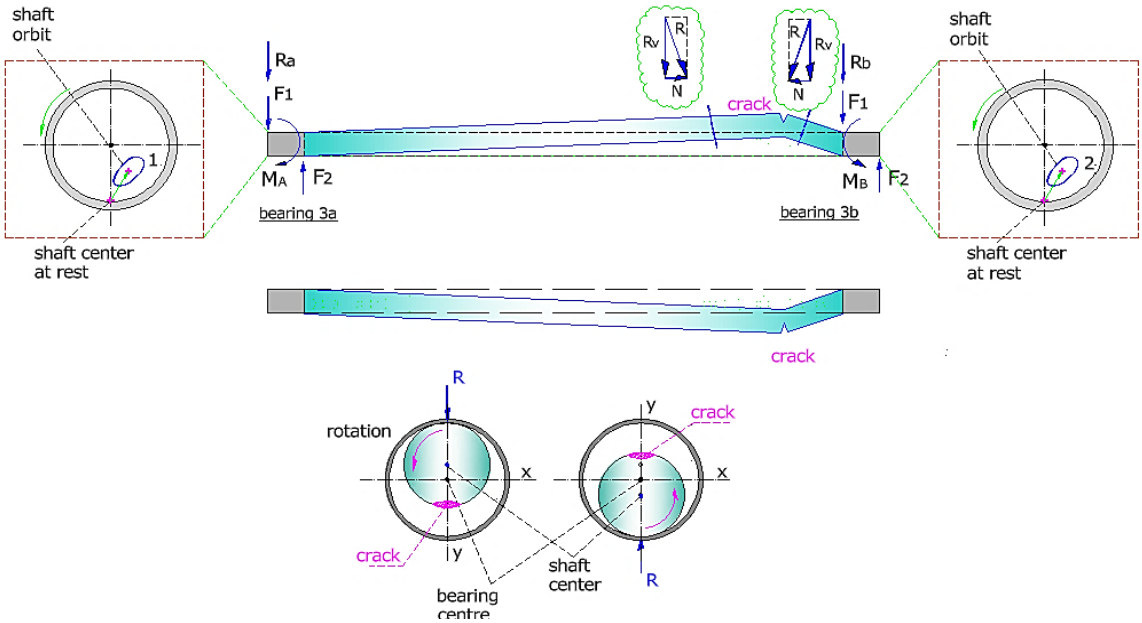

Figure 5: Crack shaft

Several other malfunctions can cause in a machine similar vibrational symptoms as under a shaft crack. There will therefore be three differentiated characteristics in the presence of the crack in the cross-section of the shaft, which are:[10]

- Unexplained changes in the response 1X shaft relative lateral vibration amplitude and phase at the operating speed.
- Changes of the “slow roll” vector on startup and shutdown.

- The apparition of response 2X vibration at the operating speed but particularly on startup and shutdown and resonant frequencies.
- Concurrency in the 1X and 2X response.
- Little or no axial vibration.
- Same response in all directions.
- Decrease in dynamic stiffness in the direction of the crack.

The most convenient transducers to detect cracking in a shaft, at low speeds and even in the symptom of "slow roll" at machine stop are induction or proximity transducers that measure the relative movement between the rotor and the stator, using measurement at 90º in vertical and horizontal directions[11].

In this study, however, we will focus on the study of the decrease in shaft stiffness.

2.1 Shaft detection using transient data

The Figure 6shows a spectrum cascade of lateral vibration during a startup of the rotor with a shaft crack, on whose shaft a transverse crack of 6 mm depth has been made, in starting point, and which will be similar in the two X, Y directions, that is, for the two transducers 9H and 9V, since as mentioned, in this case on the mechanical seal, to make the increase in amplitude more significant. The crack and its effects are internal to the shaft and rotate with it. The solution of the equations is similar: [12]

$$\begin{aligned} x(t) &= A_{0x} + A_1 \cos(\omega\, t + \alpha_1) + A_2 \cos(2\, \omega\, t + \alpha_2) \\ y(t) &= A_{0y} + A_1 \cos(\omega\, t + \alpha_1) + A_2 \cos(2\, \omega\, t + \alpha_2). \end{aligned} \tag{2}$$

The 2X response appears in both directions (amplitude A_2 and phase angle α_2); A_{0x} and A_{0y} also appear in the two planes of each transducer, which is the static displacement of the center of the shaft, caused by the curvature of this crack, accompany it in its rotation and are therefore present in all directions, although due to gravity, they will be more significant in the vertical axis, but they will have the following characteristics:

- Concurrency in the 1X and 2X response.
- When the rotative speed is 1090 rpm, which is speed that matches at a half of the resonance speed (2180 rpm), the 2X response has a resonance and increase a lot the amplitude.
- When the speed approaches the first and second resonances, the 1X response becomes dominant over the 2X.

The signal obtained from the cascade spectrum by the proximity transducers does not provide data on the phase changes, so it is represented in this Figure 6 orbit describing the shaft taken by two proximity transducers at 90º, that is useful for showing a shaft crack:

- In the speed of rotor equal to 0,5ωresthe orbit describes a typical inside loop created by 1X small response and high 2X response with little phase difference. [13]
- In the speed of rotor equal to 0,5ωres, there is a clear and significant increase in the 2X response, even in some of the 3X response, as a distinct symptom of a crack in the shaft.
- A clear example of the existence of a transverse crack in the shaft is the random change in amplitude and phase of the 1X response.
- Orbits with internal loops.
- When speed approaches the first and second resonance, the synchronous 1X component is dominant.

The approximate solution of the nonlinear equations (1) has assumed the following, shows in the Figure 6:

- In the 1X zone of rotational speed,$\omega \cong \left[(v_\xi + v_\eta)/2\right]$, the 1X harmonic response dominates.
- In the 2X zone of the rotational speed,$\omega \cong \left[(v_\xi + v_\eta)/4\right]$, the 2X harmonic response plus static displacement dominate.
- Other harmonics are neglected. [14]

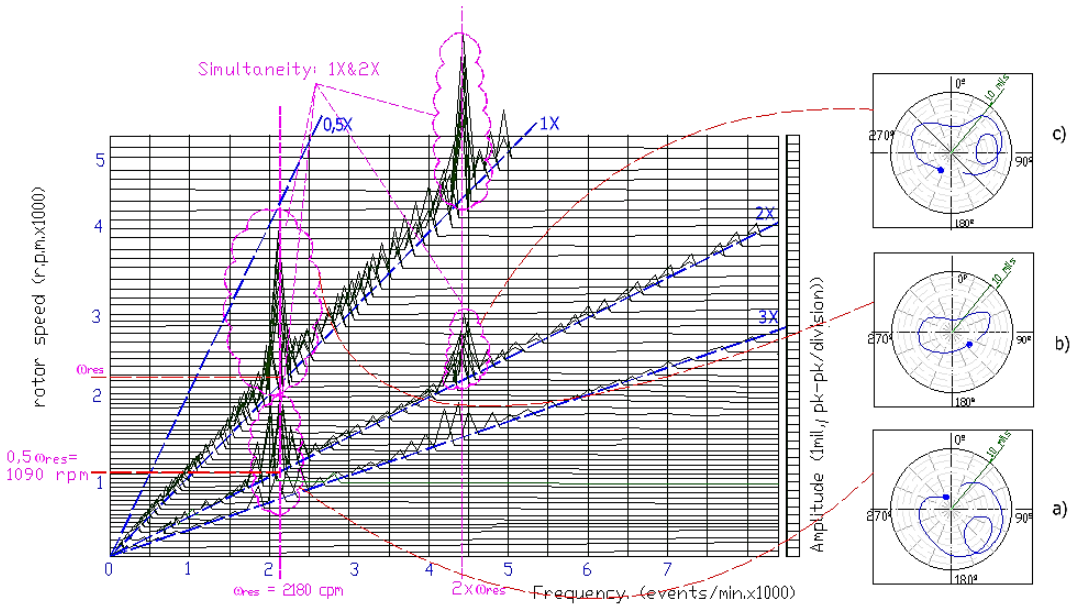

Figure 6: Spectrum cascade of lateral vibration with a shaft crack, Transductor 3bV

Another very interesting transient to see the existence of a transverse crack in the shaft is the Bode diagram according to the Figure 7. This figure shows this Bode diagram (in blue) for the rotor without transverse crack in the shaft, with a only first natural frequency at 2180 rpm for the 1X syncronous vibration and nothing in 2X response.

In the rotor, after practicing the 6 mm crack on the shaft, a vertical load is also introduced by the springs "5" of the Figure 4, to make the effect of the crack more significant. You can also see the data obtained from the 3bV vertical transducer (in green), which is higher than the horizontal transducer due to the effect of the rotor's gravity in the vertical direction and as can be seen in the red graph.

It is also observed, in this Figure 7how with the crack a resonance is produced in the 1X response and another at 2X, both at a somewhat lower value than the original ones of 2180 rpm, due to the decrease in the rigidity of the rotor, according to equation (3), where if the mass does not vary it is obvious that in order to reduce the frequency of resonance, the rigidity must decrease. The starting response of the 9V vertical transducer is graphed on the seal in red, once the determined unbalance weight and the aforementioned vertical radial load have been entered, in order to better see the increase in vibration in the 2X response.

$$\omega_{res} = \sqrt{K/M} \tag{3}$$

When signals are introduced into an oscilloscope, the orbit described by the center of the shaft inside the bearing or seal shall be presented[15]. The shape of our orbits as at low revolutions an external loop appears, but as these rpm increase and especially in the resonance zones, the orbit becomes more circular, as corresponds to a transverse crackin the shaft that gives the same signal in all directions, in addition to now presenting an internal loop, consequent with the important presence of the 2X response that is greatly amplified with a significant phase change. The internal loop is caused by forward precession of 2X component when a resonance occurs.[16]

Another characteristic of the crack is the appearance of the "slow roll" or displacement of the center of the shaft at zero revolutions, as can be seen in the Figure 7, Figure 9 and Figure 10.

A rotor with an asymmetric stiffness and a radial side load force, rotating at a speed near half of any resonant frequency can experience high 2X vibration amplitude and 2X phase shift. The 2X effect is increased when the 2X response occurs at a resonant frequency (Figure 7. Bode plot. 1X and 2X response. 3b bronze bearing and seal.)

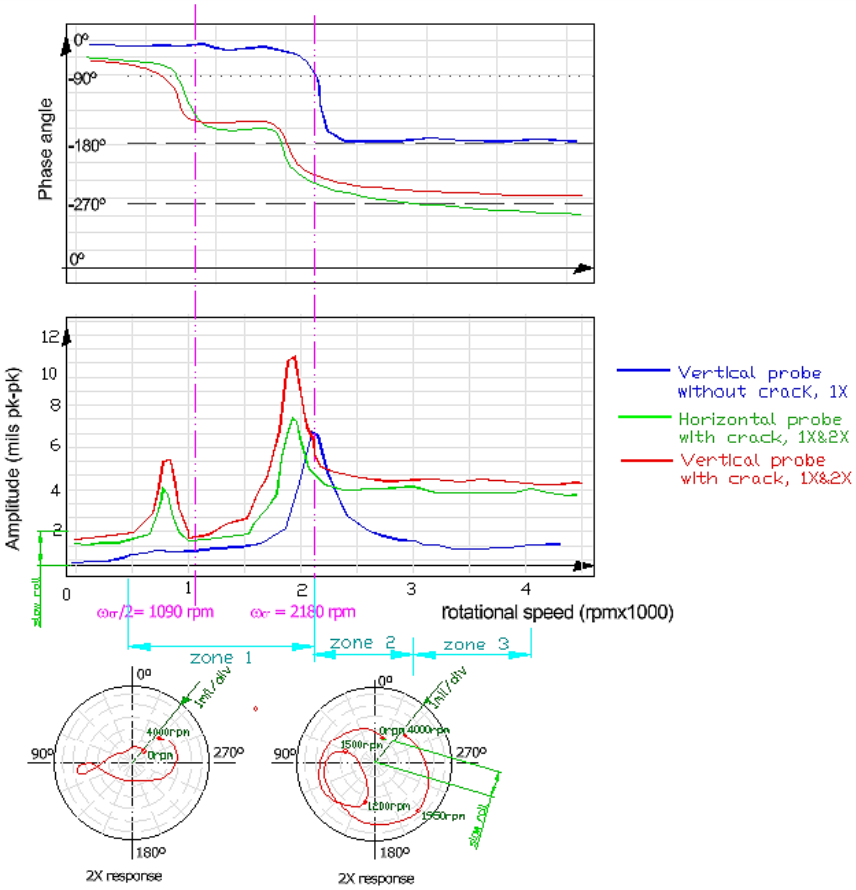

Figure 7: Bode plot. 1X and 2X response, 3b bronze bearing and seal

2.2 Dynamic stiffness

As already mentioned, this study is particular in the calculation of the dynamic stiffness of the rotor. The axis containing the crack has lower rigidity than the other axis, so in the Figure 1:

$$\begin{matrix} I_\eta < I_\xi \\ Stiffness\colon\ \ k_\eta < k_\xi \end{matrix} \tag{4}$$

In accordance with this decrease in the stiffness of the axis "η" containing the crack, it is indicated in the Figure 8 the amplitude and phase versus frequency of the 2X response for different values of the stiffness ratio.[9]

The vibration is simply the answer to a disturbance condition in a machine. It is the relation of the forces acting on the machine and its stiffness:

$$Vibration(Response)\vec{R} = \frac{Force\vec{F}}{DynamicStiffness(Restraint)\vec{K}_{DS}}$$

$\vec{R}$ = The rotor system Dynamic Stiffness is as follows, for a rotor with bronze bearings[17]:

$$\vec{K}_{DS} = (K - M\Omega^2) + jD\Omega$$

A synchronous excitation force is introduced by an imbalance of mass in the rotor; this means that the force of the inlet has the same frequency as the speed of the rotor. This imbalance causes a centrifugal force: $\vec{F} = \overrightarrow{(mr_u\Omega^2)\angle\delta}$; m, unbalance mass; r_u unbalance radius; Ω rotative speed and δ phase lag of the unbalance mass:

$$\vec{R} = \frac{\overrightarrow{(mr_u\Omega^2)\angle\delta}}{\overrightarrow{[K - M\Omega^2] + j\,[D\Omega]}} \tag{5}$$

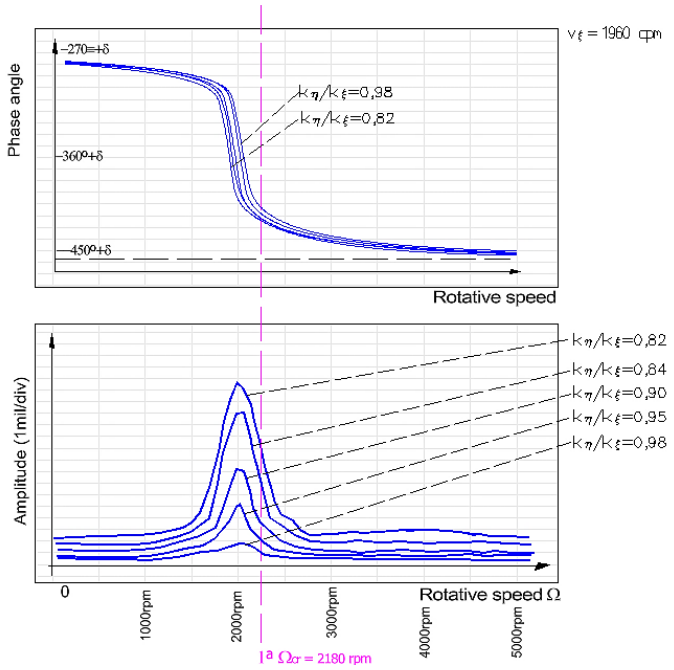

Figure 8: Bode plots. 2X filtered response, 3b bronze bearing

In classical rotor dynamics for laterally isotropic systems, in bronze bearing, the *Direct Dynamic Stiffness* (K_D) and the *Quadrature Dynamic Stiffness* (K_Q) are:

$$K_D = K - M\Omega^2 \;\; ; \;\; K_Q = D\Omega$$

The *direct dynamic stiffness* according to the frequency "Ω" is a parabola and the *quadrature dynamic stiffness* according to the frequency "Ω" is a straight line that crosses the vertical axis on its negative side. The Dynamic Stiffness is a function of the excitation frequency, and it is useful to see how Dynamic Stiffness changes as a result of perturbation frequency [18].

2.2.1 Calculation of Dynamic Stiffness

It has already been said which an important characteristic of the crack is the reduction of the stiffness of the shaft and consequently of the resonance frequency, as already mentioned.

To calculate the dynamic stiffness, obtaining some graphs like those transit date of the Figure 9. In this case, the displacement of the shaft centre at "0" rpm (slow roll) is already observed, because of the curvature produced by that crack. The orbits are also clearly seen in a circular form, with an internal loop, which is identified with 1X and 2X responses and which may be a clear characteristic of a transverse crack in this shaft[19], [20].

It is also characteristic of a crack in the shaft that the answer of the Bode diagram in the Figure 9, the resonances are shown at a rotational speed (ω_1 and ω_2) lower than the original Ω_{crit}= 2180 rpm and $\Omega_{crit}/2$.

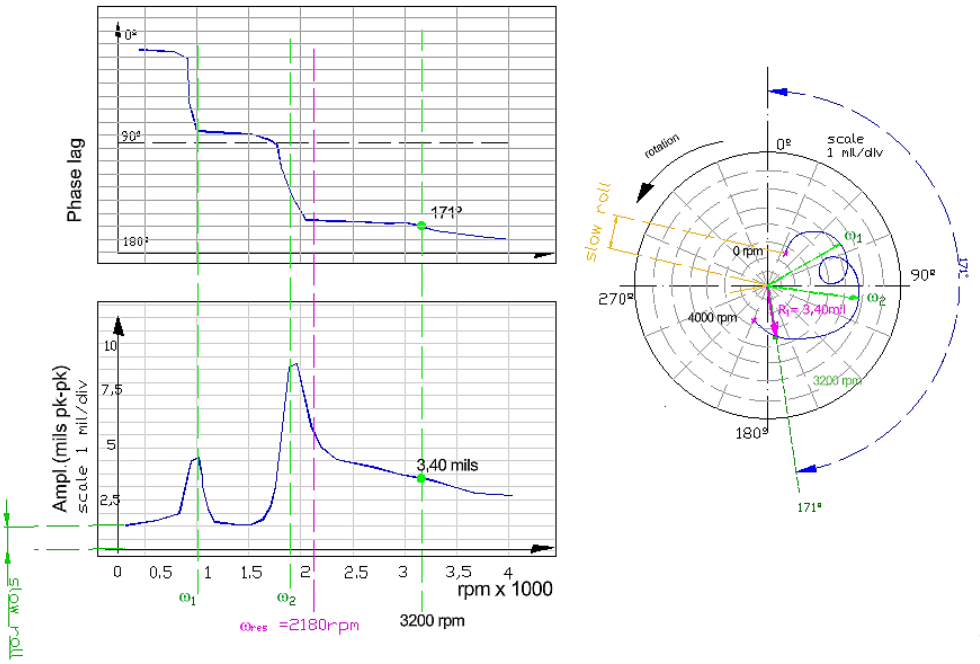

Figure 9: Response data with crack. 3b bronze bearing

As a point of data collection and comparison, 3200rpm is chosen. The response obtained in polar coordinates is R_1 = 3,40 mils (1 mil = 0,0254 mm) at 171º with respect to the upper point of the Nyquist diagram marked with 0º (Figure 9), which in rectangular format is: +0,73- j 3,32 mils pp.

Next, a new start analysis will be performed after adding an unbalanced mass known in module and direction: 0,1 gr. in a position of 90º and at a radial distance of 50 mm in the disk "6" of the Figure 4, and in addition an external force of 50N is introduced by the springs of the "5" disc of this Figure 4 in order to force and propagate the 6 mm crack introduced at the beginning of the study. The corresponding graphs to be obtained are now indicated in Figure 10 in polar coordinates, at the same speed of3200 rpm, which indicates a vibration response($R_1 + R_2$)of 4,01mils in the 197° direction.

This new response ($R_1 + R_2$), is the sum of the response with crack of 6 mm of the origin (R_1) plus the one that now corresponds to the sum of the unbalance weight determined, in addition to having introduced an external force of 50N: (R_3) = $R_1 + R_2$ = 4,01 mils at 197º, which in rectangular form is:1,10 -j3,86 and therefore the response that is due exclusively to the weight of added imbalance (R_3), is calculated as subtraction of both vectors in the rectangular form, whose vector representation can also be observed in the Figure 10, Figure 11 and Table 1:

Table 1. Response due to determined weight alone

	Polar	Rectangular
$R_1 + R_2$ =	4,01∠197º	-1,10 - j 3,86 mils pp
$-R_1$=	3,40∠171º	+0,73 - j 3,32 mils pp
R_3 =	1,70∠ 255º	-1,59 – j 0,60 mils pp

The force that is applied, with that weight of imbalance determined (0,1gr∠90º) at the test speed of 3200 rpm (335,10rad/s), is:

$$\vec{F} = mr_u\Omega^2 e^{j\delta} =$$

$$\left(0{,}1 * 10^{-3} kg \left(N/m/s^2\right)\right) * (50 * 10^{-3}\, m) * \left(335{,}10\ rad/s\right)^2 \angle 90º = 0{,}561460 * 10^{-6}\ N \angle 90º \text{ p.p.}$$

And the calculation of the dynamic stiffness, which is performed for a zero to peak amplitude, forces to divide the previous imbalance force p.p. for 2:

R_3 = (1,70 mils / 2) ∠255º = 0,85 mils ∠ 255º = 0,0216*10^{-3} m ∠255º

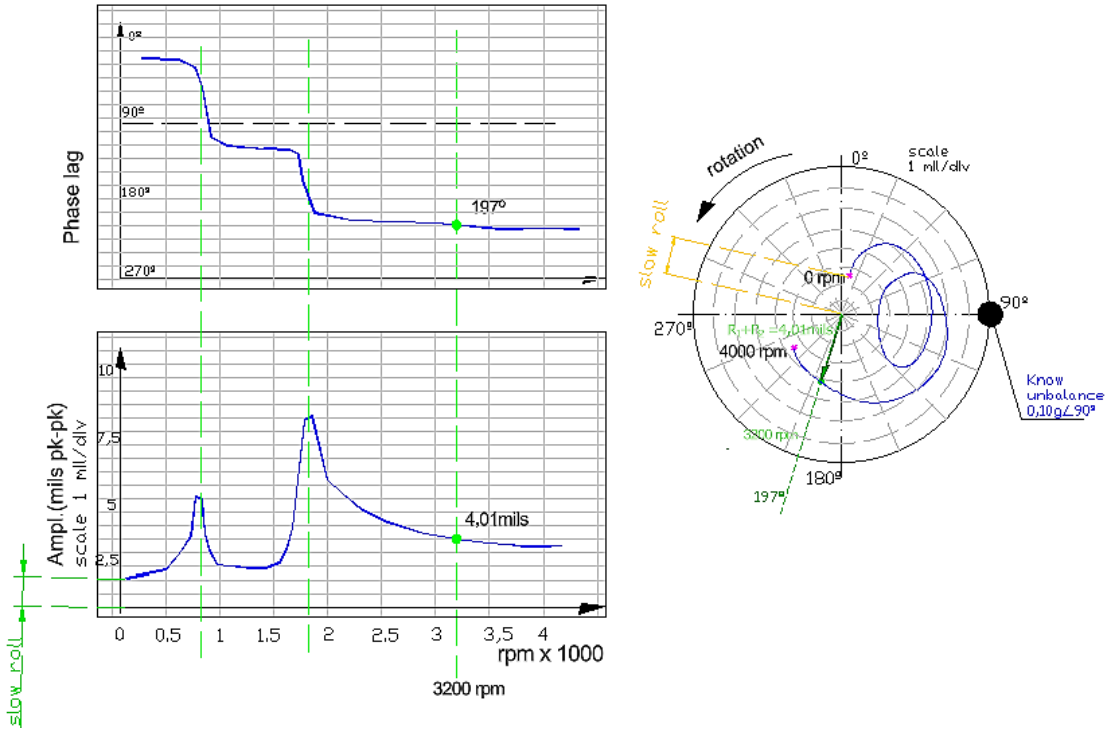

Figure 10: Test with crack and imbalance of determined mass. 3b bronze bearing.

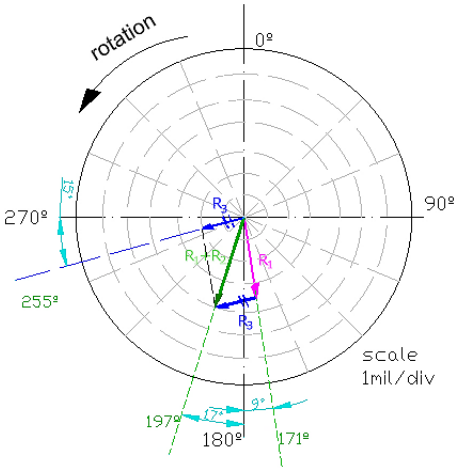

Figure 11: New response vector witch crack and unbalanced. 3b bronze bearing

The response R_3, represented in a polar diagram like the one in Figure 11, indicates its amplitude and phase: $(\vec{R}_1 + \vec{R}_2) - \vec{R}_1 = \vec{R}_3$, so it can be expressed exponentially as $\vec{R}_3 = Ae^{j\alpha}$, where "A" is the amplitude of the response and "α" the phase angle, being the disturbing force of the controlled imbalance: $\vec{F} = Fe^{j\delta}$

$$\vec{K}_{DS} = \frac{\vec{F}}{\vec{R_3}} = \frac{F\,e^{j\,\delta}}{A\,e^{j\alpha}} = \frac{F}{A}e^{j\,(\delta-\alpha)} = \frac{F}{A}\angle -(\delta-\alpha) =$$

$$\frac{561{,}46 * 10^{-3}\ N}{0{,}0216 * 10^{-3}\ m}\angle -(90-255)º = 25993{,}52\ {}^{N}/_{m}\angle 165º = 25{,}99\ {}^{KN}/_{m}\ \angle 165º$$

The negative sign of the calculate dynamic stiffness phase angle $\{-(\delta-\alpha)\}$, is introduced because the phase angle is measured as phase lag.

- Dynamic Stiffness, real component:

$$K_D = K_{DS} * \cos\theta_k = 25{,}99 \text{ KN/m} * \cos 165^o = -25{,}10 \text{KN/m}$$

- Dynamic stiffness, imaginary component:

$$K_Q = K_{DS} * \sin\theta_k = 25{,}99 \text{ KN/m} * \sin 165^o = 6{,}72 \text{ KN/m}$$

It is necessarily knowing the reference date of the startup or shutdown. The information to calculate dynamic stiffness is obtained every time balance the machine, (2.- Experiment and Case Study, pag.4).

Different tests have to be carried out, with the same determined weight of imbalance, for example 0,1 gr∠ 90º and a radial position of 50 mm at different speeds of rotation, give rise to the responses of Figure 12: a parabola for the component of the real dynamic stiffness $K_D = K\text{-}M\Omega^2$.

In this Figure 12it is observed how this K_D component, which is determined by extending the parabola to the ordinate axis ($K_D = K - M\Omega^2$; at Ω = 0 rpm you get K_D= K), that is 15 KN/m with the propagation of the crack, thus decreasing with respect to the value of that rotor without crack of 18 KN/m obtained of the reference date. Likewise, the first natural frequency of resonance decreases of 2180 rpm (without crack, which corresponds in the Figure 12to the blue curve), to1950 rpm in this case with crack, facts that are clearly identified with the crack made and grown by the radial load.

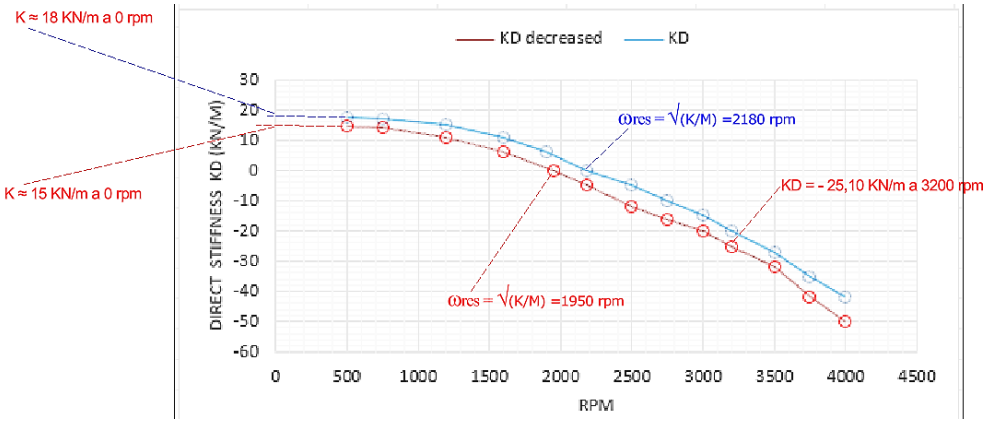

Figure 12: Dynamic Stiffness. 3b bronze bearing

The modal spring stiffness K then can be found by extending the parabola graph obtained for Z_D to the zero value of the abscissa axis Ω and, analytically, making the comparison between the two chosen points:

$\Omega_{resonance}$ = 2180 rpm	Ω_{point}= 3200 rpm
$K_D = K - M\Omega_{res}^2 = 0$	$K_D = K - M\Omega_{3200}^2$

that give us two equations with two unknowns, among which the parameter of the mass "M" is eliminated, in addition to using the values obtained previously, coinciding with the value of K obtained from Figure 12.

$$\frac{K}{\Omega_{res}^2} = M = \frac{1}{\Omega_{3200}^2}[K - K_D] \;\; ; \quad K = \frac{K_D}{\left(1 - \frac{\Omega_{3200}^2}{\Omega_{res}^2}\right)} = \frac{18 * 10^3 \, N/m}{\left(1 - \frac{335.10^2}{228.21^2}\right) rad/s} = 15 * 10^3 \, N/m$$

The modal damping "D" is deduced from the expression of the imaginary component of the dynamic stiffness:

$$K_Q = D(1 - \lambda)\Omega_{3200}$$

The coefficient "λ" is estimated, in this case the "test rotor" with a bronze bearing, λ = 0:

$$D(1 - \lambda) = \frac{K_Q}{\Omega_{3200}} = \frac{6727{,}61 \; N/m}{335{,}10 \; rad/s} = 20{,}07 \, {}^{N}/_{m/s} \; ; \quad para \; \lambda = 0, D = 20{,}07 \, {}^{N}/_{m/s}$$

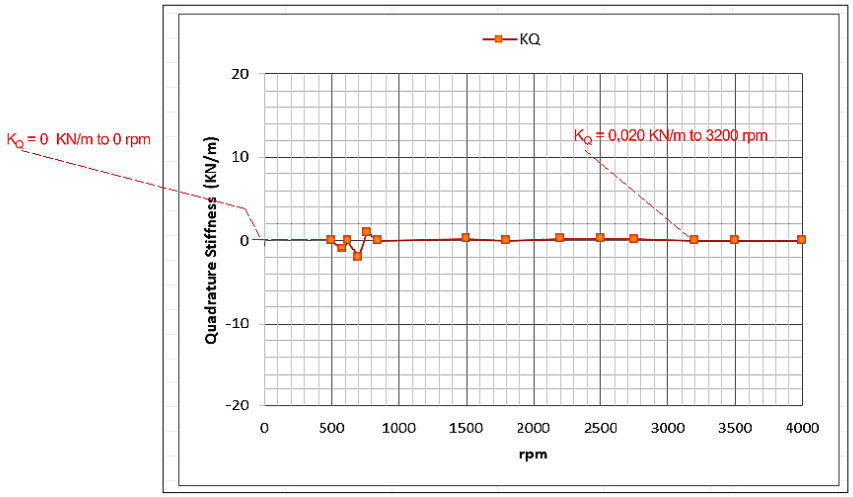

Figure 13: Dynamic stiffness. Imaginary component, 3b bronze bearing

By performing the calculation for several other points in addition to the one corresponding to 3200 rpm, the graph of the magnetic component of the dynamic stiffness will be obtained, which will be a line according to the Figure 13, in whose expression for a bronze bearing, where λ is zero, is $K_Q = D\Omega$ and for the zero speed it is also zero.

This means that, for this bronze solid bearing rotor, the damping is almost zero.

3. Conclusions

It has been studied a rotor model of 2 degrees of freedom, with solid bronze bearings. which has been made a maximum transverse crack of 10% of its diameter, in addition to introducing a mass imbalance and a vertical radial load to cause the propagation of this crack. The rotor under consideration is horizontal, so the force of gravity will also act and add to the vertical load for that crack propagation.

The 1X synchronous response and the 2X non-synchronous response are studied and analyzed and it is observed how the vibration response is increased in these two responses due to the crack and in what mannerit is related to the stiffness coefficient between the axis containing the crack and its perpendicular, which does not include the damping and asymmetric stiffness of the rotor base.

There are many symptoms of a transverse crack in the shaft, such as: changes in the 1X response and increased amplitude; appearance of the "slow roll"; erratic response to balancing; center of the shaft in simultaneous quadrants; 2X response important with amplitude and phase changes; 2X response in resonant frequency and in the value of its half; orbits with internals loops; 2X response increases over time; symmetry of response in the two transducers installed at 90º; orbits of almost circular shape; concurrency of 1X and 2X responses, but in this study, it is particularized in the change of dynamic stiffness, which decreases significantly, since a curvature in the shaft or other anomalies would not result in a clear difference in stiffness between the shaft containing the crack and the other perpendicular, according to the study case in this work. The instrumentation and diagnostic methodology is now available to detect shaft cracks before catastrophic failure of the machine occurs and is effective for early detecting shaft cracks.

4. References

[1]. O. Jun, H. Eun and Y. Earmme, “Modelling and vibration analysis of a simple rotor with breathing crack.,” Journal of Sound Vibration., vol. 2, no. 155, pp. 273-290, 1993.

[2]. J. Wauer, “On the dynamics of cracked rotors: A literature survey,” Applied Mechanics Reviews, vol. 43, no. 1, pp. 13-17, 2009.

[3]. J. Wauer, “On the dynamics of cracked rotors: A literature survey,” American Society of Mechanical Engineers, vol. 43, no. 1, pp. 13-17, 2009.

[4]. B. Warda and A. Chudzik, “Effect of ring misalignment on the fatigue lif of yhe radial cylindrical roller bearing,” International Journal of Mechanical Sciences, vol. 111, no. March, pp. 1-11, 2016.

[5]. T. Patel and A. Darpe, “Vibration response of coupled rotor systems with crack and misalignment,” Mechanical Engineering Sciences, vol. 225, pp. 700-713, 2016.

[6]. P. G. L. Dal Bo, "Energy harvesting with electromagnetic and piezoelectric seismic transducers: Unified theory and experimental validation," Journal of Sound and Vibration, vol. 433, no. https://doi.org/10.1016/j.jsv.2018.06.034, pp. 385-424, 2018.
[7]. Bently Nevada. Rotor Kit., 2016.
[8]. C. Hatch, R. Jesse and J. Whiteley, "Machinery Diagnostics Dynamic Stiffness in whirl and whip," Bently Nevada Technical Training Department, Skelmersdale, UK, 2016.
[9]. A. Muszynska, "6.5.2 Model of a Cracked Rotor Supported by Isotropic Elastic Supports," in Rotordynamics, Columbus, Ohio. USA, Taylor & Francis, 2005, pp. 785-824.
[10]. N. P. V. Kushwaha, "Modelling and analysis of a cracked rotor: a review of the literature and its implications. https://doi.org/10.1007/s00419-020-01667-6," Springer Nature , Vols. 2020-06, pp. 1215-1245, 2020.
[11]. A. P. I. (API), No contacting vibration and axial position monitoring system. Standard number 670., New York: American Petroleum Institute (API), Fifth edition 2014.
[12]. J. Y. W. Y. Chaozhong Guo, "Crack detection for a Jeffcott rotor with a transverse crack: An experimental investigation," Mechanical Systems and Signal Processing, vol. 83, no. January, pp. 260-271, 2017.
[13]. P. M. A. B. D. E. D. Goldman, "Application of perturbation methodology and directional filtering for early rotor crack detection," in ASME International Gas Turbine & Aeroengine Congress & Exhibition., Indianapolis. USA, 199.
[14]. B. Grabowski, "Shaft vibrations in turbomachinery excited by cracks," A&M University workshop Proceedings, Texas, USA, 1982.
[15]. B. L. A. Fraga De Cal, "Capítulo 1. Introducción al movimiento de los mecánicos.," in Diagnóstico de averías fundamentales en máquinas rotativas por análisis de vibraciones., A Coruña. Spain, A Coruña University, 2023, pp. 31-38.
[16]. D. E. Bently, "Shaft Centerlines," Orbit. Bently rotor dynamics., no. April, pp. 3-6, 1989.
[17]. L. Tam, A. Przekwas, R. Hendricks and M. Braun, "Numerical and Analytical Study of Fluid Dynamic Forces in Seals and Bearings.," Journal of Vibration, Acoustics, Stress, and Reliability en Design. Trans of the ASME., vol. 110, no. 3, pp. 315-325, 1988.
[18]. E. Jang, Y. Park, C. Kim and A. Muszynska, "Identification of the quadrature resonances using modal nonsynchronous perturbation testing and dynamic stiffness approach for an anisotropic rotor system with fluid interaction," International Journal of Rotating Machinery, vol. 2, no. 3, pp. 187-199, 1996.
[19]. P. Goldman and A. Muszynska, "Dynamics of rotors with transverse cracks," in Proceedings of the 12º Machinery Prevention Technology Conference, Virginia, USA, 1997.
[20]. G. E. Company, "Synchronous Dynamic Stiffness," in Manual Part Number: SM00025version 9. Machinery Management and Diagnostics., Minden, Nevada. USA, Bentley Nevada Corporation, 2012, pp. 704-737.

